

QCD analysis of Lambda hyperon production in DIS target-fragmentation region

Federico Alberto Ceccopieri^{(a,b)*} and **Davide Mancusi**^{(a,c)†}

^(a)*IFPA, Université de Liège,
Allée du 6 août, Bât B5a, 4000 Liège, Belgium*

^(b)*Université Libre de Bruxelles,
Boulevard du Triomphe, 1050 Bruxelles, Belgium*

^(c)*CEA, Centre de Saclay, IRFU/Service de Physique Nucléaire,
F-91191 Gif-sur-Yvette, France*

Abstract

We consider Lambda-hyperon production in the target-fragmentation region of semi-inclusive deep-inelastic scattering within the framework of fracture functions. We present a first attempt to determine the flavour and energy dependences of these non-perturbative distributions through a simultaneous QCD-based fit to available neutral- and charged-current semi-inclusive-DIS cross sections. Predictions based on the resulting nucleon-to-Lambda fracture functions are in good agreement with data and observables not included in the regression. The successful prediction of the Q^2 dependence of the Lambda multiplicity notably represents the first validation of the perturbative framework implied by fracture functions.

*Email address : federico.ceccopieri@hotmail.it

†Email address : davide.mancusi@cea.fr

1 Introduction

It has been known for a long time [1] that in hadronic collisions the longitudinal momentum spectrum of particles produced in target fragmentation crucially depends on the difference of the valence-parton composition of the initial- and final-state particles. In particular, only an initial-state particle whose valence-quark flavour content is almost or totally conserved in the scattering can be a leading particle in the final state, *i.e.* carry a substantial fraction of the incoming projectile energy. Counting rules connect the differences in the valence-parton composition of initial- and final- state particles with the shape of longitudinal momentum spectrum of the latter. Leading particles in the final state are typically characterised by large longitudinal momentum fractions and very small transverse momenta with respect to the collision axis, a typical regime dominated by soft QCD dynamics where standard perturbative techniques cannot be applied.

The leading particle effect manifests itself in reactions involving at least one hadron in the initial state. Quite interestingly, it also appears in processes which involve point-like probes, such as Semi-Inclusive Deep Inelastic Scattering (SIDIS). At variance with the hadronic collisions discussed above, such process involves a large momentum transfer. Therefore, thanks to the factorisation theorem, the short-distance cross section can be calculated by using perturbation theory, while soft QCD effects are effectively encoded by universal parton distributions and fragmentation functions. The properties of these non-perturbative objects are generally extracted from the so called current-fragmentation region, *i.e.* the phase-space region in which the struck parton hadronises.

The target-fragmentation region is instead sensitive to the hadronisation properties of the coloured spectator system which results from the removal of one parton from the incident nucleon by the virtual probe. For these reasons, the description of particle production in this particular region of phase space through standard perturbative calculations based on parton distributions and fragmentation functions will fail when compared to data. The description can be improved only with the introduction of new non-perturbative distributions which encode these peculiar aspects of soft QCD dynamics.

This was early realised in Ref. [2] where the authors introduced the concept of fracture functions. These distributions simultaneously encode information on the interacting parton and on the fragmentation of the spectator system. Although intrinsically of non-perturbative nature, the scale dependence of such distributions can be calculated within perturbative QCD [2]. Fracture functions obey in fact DGLAP [3] inhomogeneous evolution equations which result from the structure of collinear singularities in the target-fragmentation region [2, 4]. Moreover, a dedicated factorisation theorem [5, 6] guarantees that fracture functions are universal distributions, at least in the context of SIDIS.

The phenomenology which makes use of all these concepts is still confined to the study of hard diffraction in DIS. Within this framework, in fact, no analysis has been attempted for particles other than proton in the final state. It is well known, however, that Lambda hyperon production in SIDIS is mainly concentrated in the target-fragmentation region since Lambdas show a significant leading particle effect.

In this paper we describe how a variety of Lambda leptonproduction cross sections can be simultaneously described within the fracture-function approach, if these non-perturbative distributions are modelled at some low scale and their free parameters determined by a fit to the

available data. The rather scarce Lambda leptonproduction data in general do not allow to directly verify the leading-twist nature of this type of processes, which is implicitly assumed in the fracture-function framework, nor allow to test the scale dependence embodied by their specific evolution equations. In this respect, both the formalism and the model presented in this paper require more experimental information for a conclusive validation. We believe, however, that a quantitative tool that is able to reproduce many aspects of the existing data may further stimulate both theoretical and experimental activity. As a by-product, the model will give us the first insights on the flavour and energy dependences of the fragmentation properties of the spectator system into Lambda hyperons.

The paper is organized as follows. In Section 2 we briefly recall SIDIS cross sections and fracture-function properties. In Section 3 we discuss specific features of the data sets and observables used in the analysis. In Section 4 we describe a simple model for Lambda fracture functions and in Section 5 we provide and discuss the results of our fit. In Section 6 we compare the model predictions with data and observables not used in the fit. In Section 7 we summarise our results.

2 Semi-Inclusive DIS in the target-fragmentation region

The deep inelastic scattering cross section of a lepton l off a proton p with four-momenta k and P , respectively, is described in terms of the lepton variables:

$$x_B = \frac{Q^2}{2P \cdot q}, \quad y = \frac{P \cdot q}{P \cdot k} = \frac{Q^2}{s_h x_B}, \quad Q^2 = -q^2, \quad (1)$$

where k' and $q = k - k'$ are the outgoing lepton and virtual photon four-momenta, respectively, $s_h = (P + k)^2$ is the centre of mass energy squared and $W^2 = s_h y(1 - x_B) + m_p^2$ is the invariant mass squared of the final state, with m_p^2 being the proton mass. The additional invariant [4]

$$z_h = \frac{P \cdot h}{P \cdot q} = \frac{E_h}{E_P(1 - x_B)} \frac{1 - \cos \theta_h}{2}, \quad (2)$$

is often used to specify the kinematics of final state hadron with four-momentum h , where E_h and θ_h are the detected hadron energy and angle respectively defined in the virtual photon-proton centre of mass frame. The variable z_h is however not adequate to describe target fragmentation, since both soft hadron production ($E_h \simeq 0$) and hadron production in the target-remnant direction ($\theta_h \simeq 0$) both yield a vanishing value of z_h . We therefore consider cross sections differential either in the scaled hadron energy variable z or ζ [4]

$$z = \frac{\zeta}{1 - x_B}, \quad \zeta = \frac{E_h}{E_P}, \quad (3)$$

again defined in the γ^*p centre of mass frame. It follows from eq. (3) that final-state hadrons are detected with a fraction $z \in [0, 1]$ of the spectator energy $E_P(1 - x_B)$. In the following we will analyse data presented in term of Feynman's variable

$$x_F = \pm \left(z^2 - \frac{4m_T^2}{W^2} \right)^{\frac{1}{2}}. \quad (4)$$

We adopt the convention that, in the γ^*p frame, negative values of x_F correspond to final state hadrons moving parallel to incoming proton direction. In eq. (4) we have introduced the hadron transverse mass, $m_T^2 = m_h^2 + p_{h,\perp}^2$, defined in terms of its transverse momentum and mass squared.

In the quark-parton model, the neutral-current semi-inclusive DIS cross section for producing an unpolarised Lambda off a proton in the target-fragmentation region reads [4]

$$\frac{d^3\sigma^{lp \rightarrow l\Lambda X}}{dx_B dQ^2 d\zeta} = \frac{2\pi\alpha_{em}^2}{Q^4} JY_+ \sum_{q=u,d,s} e_q^2 \left[M_q^{\Lambda/p}(x_B, Q^2, \zeta) + M_{\bar{q}}^{\Lambda/p}(x_B, Q^2, \zeta) \right], \quad (5)$$

where $Y_+ = 1 + (1 - y)^2$. The cross section has been re-expressed for later convenience in term of the ζ variable, and the jacobian $J = \zeta[(1 - x_B)|x_F|]^{-1}$ has been explicitly indicated [7]. The latter reduces to unity in the high-energy limit and it is therefore often omitted in the literature. The neutrino- and anti-neutrino-induced charged-current semi-inclusive cross sections read respectively

$$\frac{d^3\sigma^{\nu p \rightarrow \mu^- \Lambda X}}{dx_B dQ^2 d\zeta} = \frac{2\pi\alpha_{em}^2}{Q^4} J8\eta_W \left[2(M_d^{\Lambda/p} + M_s^{\Lambda/p}) + 2(1 - y)^2 M_{\bar{u}}^{\Lambda/p} \right], \quad (6)$$

and

$$\frac{d^3\sigma^{\bar{\nu} p \rightarrow \mu^+ \Lambda X}}{dx dQ^2 d\zeta} = \frac{2\pi\alpha_{em}^2}{Q^4} J8\eta_W \left[2(M_{\bar{d}}^{\Lambda/p} + M_{\bar{s}}^{\Lambda/p}) + 2(1 - y)^2 M_u^{\Lambda/p} \right], \quad (7)$$

where the dependencies of M_i appearing in eq. (6) and eq. (7) are to be understood as in eq. (5). The factor η_W is defined in terms of the Fermi constant G_F , the W -boson mass M_W^2 and the electromagnetic coupling constant α_{em} as [8]

$$\eta_W = \frac{1}{2} \left(\frac{G_F M_W^2}{4\pi\alpha_{em}} \frac{Q^2}{Q^2 + M_W^2} \right)^2. \quad (8)$$

As appropriate for a lowest-order calculation, we have assumed a vanishing longitudinal structure-function contribution in all formulas. We have further neglected charm quarks contribution.

In eqs. (5, 6, 7) the production of unpolarised Lambdas in the remnant direction is described by fracture functions $M_i^{\Lambda/p}(x, \zeta, Q^2)$ [2]. These distributions express the probability to find a parton of flavour i with fractional momentum x_B and virtuality Q^2 conditional to the detection of a target Lambda with a fraction ζ of the incoming proton energy. The scale dependence of fracture functions is given by the following evolution equations [2]

$$\begin{aligned} \frac{\partial M_i^{\Lambda/p}(x_B, \zeta, \mu^2)}{\partial \log \mu^2} &= \frac{\alpha_s(\mu^2)}{2\pi} \int_{\frac{x_B}{1-\zeta}}^1 \frac{du}{u} P_i^j(u) M_j^{\Lambda/p}\left(\frac{x_B}{u}, \zeta, \mu^2\right) + \\ &+ \frac{\alpha_s(\mu^2)}{2\pi} \int_{x_B}^{\frac{x_B}{x_B+\zeta}} \frac{du}{x_B(1-u)} \hat{P}_i^{j,l}(u) f_{j/p}\left(\frac{x_B}{u}, \mu^2\right) D_l^{\Lambda}\left(\frac{\zeta u}{x_B(1-u)}, \mu^2\right), \end{aligned} \quad (9)$$

where $P_i^j(u)$ and $\hat{P}_i^{j,l}(u)$ are the regularised [3] and real [9] Altarelli-Parisi splitting functions, respectively. Eq. (9) describes both processes which contribute to Lambda production in the

Reaction type	$\langle E_i \rangle$ (GeV)	$\langle W^2 \rangle$ (GeV ²)	$\langle Q^2 \rangle$ (GeV ²)	$\langle x_B \rangle$	Λ rates (%)
νp [12]	50.0	-	-	-	7.0 ± 1.2
νn [12]	50.0	-	-	-	7.0 ± 0.8
νp [13]	42	34.7	8.7	0.2	5.2 ± 0.3
$\bar{\nu} p$ [13]	38.5	20.4	5.2	0.2	5.7 ± 0.4
μp [14]	280	130	12	0.11	-
μD_2 [14]	280	130	12	0.11	-
μD_2 [15]	490	292	8.6	0.036	7.8 ± 1.6

Table 1: Data sets used in the present analysis. $\langle E_i \rangle$ is the average energy of the incoming lepton. Average kinematics and production rates for the various data set, when available, are indicated.

target-remnant direction. The homogeneous term on the right hand side of eq. (9) takes into account the effects of collinear parton radiation by the struck parton i while the Lambda originates from the fracture function itself. The inhomogeneous one instead takes into account the possibility that the detected Lambda results from the fragmentation of the radiated parton l , emitted collinearly to the incoming parton j . This term in fact is a convolution of parton distributions $f_{j/p}(x_B, Q^2)$ and fragmentation functions $D_l^\Lambda(z, Q^2)$.

Given the explorative purpose of this analysis, we use leading-order formulas for semi-inclusive cross sections and consistently solve fracture-function evolution equations at leading logarithmic accuracy. We note, however, that the full formalism is available at next-to-leading-order accuracy for both unpolarised [4] and polarised [10, 11] processes.

3 Data sets and Observables

The data used in the present analysis come from a variety of fixed-target experiments. We include neutrino and anti-neutrino SIDIS data which are crucial in providing minimal quark-flavour discrimination. In particular, the stringent cuts ($x_B > 0.2$ and $W > 4$ GeV) in data from Ref. [12] enhance the sensitivity to valence-quark fracture functions; data from Ref. [13] are expected to be an admixture of valence and sea contributions and therefore constrain the relative normalisations of the respective fracture functions. We further include in the fit neutral-current SIDIS data at higher beam energy presented in Refs. [14, 15] in order to provide the necessary information about the energy dependence of the cross sections and therefore on the x_B -dependence of fracture functions.

Some care should be used in the selection of the targets. Since charged-current cross sections are significantly lower than neutral-current ones, many experiments have used nuclear targets. The first consequence is that nuclear corrections to fracture functions might be accounted for. Even more important for the purposes of this analysis, the fragmentation process itself might be affected by the nuclear medium, both in the current [16] and in the target [17] fragmentation region. In particular, it has been recently reported in Ref. [17] that strange-particle yields in neutrino-nuclei interactions are enhanced in the target region, probably due primary particles

re-interaction with the nuclear medium. Since the particle yields show a mild power dependence on the atomic number of the target, we include in the present analysis only proton- and deuteron-target data.

We would like to mention two effects which might affect the absolute normalisations of the various data sets. The first one is related to the definition of fracture functions. Many analyses quoted in Tab. (1) have estimated the contributions to the Lambda yield coming from the decay of higher-mass resonances. When not otherwise stated in the original publications, we interpret the published data as referring to an inclusive Lambda sample, that is the sum of promptly produced Lambdas and Lambdas coming from the decay of higher-mass resonances, corrected for unseen decay modes (a typical example is the $\Sigma^0 \rightarrow \Lambda \gamma$ decay mode discussed in Ref. [14]). The decay of higher-mass resonances in fact happens at time scales much larger than the ones typical of perturbative processes and their effects will be effectively incorporated in fracture functions.

The second issue is related to the contamination of the Lambda yield by secondary Lambdas produced by the re-interaction of primary pions with detector material. This effect has been intensively studied in Ref. [18] and estimated to contribute up to 20% to the Lambda yield. It is unknown to us to which extent this correction has been properly estimated and applied to all data sets.

We close this Section discussing the choice and the reconstruction of the observable to be used in the fit. By definition, cross sections differential in the Lambda fractional energy are insensitive to the phase space region in which the latter has been produced. In this variable, the current- and target-fragmentation contributions overlap and the extraction of the latter therefore crucially depends on the precision with which we describe current fragmentation with available Lambda fragmentation functions. In order to overcome this problem, we consider differential cross sections in the Feynman variable x_F which offer, to lowest order, a kinematical separation of the two contributions. The use of such a variable is however not free from additional issues: Lambda-mass effects introduced via eq. (4) may be sizeable, as suggested by the values of the averaged hadronic final-state invariant mass $\langle W^2 \rangle$ quoted in Tab. (1). Such effects are however not compatible with the pQCD factorisation theorem. In the present analysis, Lambda-mass effects are therefore applied a posteriori to the Lambda leptonproduction cross sections σ^Λ , as described in Ref. [19]. The value in each x_F -bin is calculated as follows

$$\frac{1}{\sigma_{\text{DIS}}} \frac{\Delta \sigma_i^\Lambda}{\Delta x_F^i} = \frac{1}{\sigma_{\text{DIS}}} \frac{1}{\Delta x_F^i} \int dE_l \Phi(E_l) \int_\Omega dx_B dQ^2 \int_0^{1-x_B} d\zeta \frac{d^3 \sigma^\Lambda(E_l)}{dx_B dQ^2 d\zeta} \Theta^i(x_F), \quad (10)$$

where the index i labels the i -th bin and the bin-size is specified by $\Delta x_F^i = x_F^{i+1} - x_F^i$, with x_F^i representing the experimental bin-edges. Mass corrections are enforced with the kinematical constraint $\Theta^i(x_F) = \theta(x_F - x_F^i) \theta(x_F^{i+1} - x_F)$, with x_F calculated via eq. (4). The label Ω stands for the set of cuts which define the DIS selection of a given data set. The resulting differential cross sections are then normalised with respect to the inclusive DIS cross section

$$\sigma_{\text{DIS}} = \int dE_l \Phi(E_l) \int_\Omega dx_B dQ^2 \frac{d^2 \sigma^\Lambda(E_l)}{dx_B dQ^2}, \quad (11)$$

calculated with parton-distribution functions of Ref. [20]. Both cross sections are integrated over the lepton flux factor $\Phi(E_l)$ expressed in units of GeV^{-1} . For monochromatic electron and muon

beams of energy $E_{l,0}$, the latter simply reduces to $\delta(E_l - E_{l,0})$. For neutrino and anti-neutrino beams we use the flux-factor parametrisations extracted by dedicated analyses [21]. We finally note that mass-corrected distributions are derived by using eq. (3) and eq. (4) and therefore require the knowledge of the Lambda transverse momentum. From the very precise data of Ref. [18] we know that the Lambda p_t -spectrum is dominated by p_t values much smaller than its mass. We therefore approximate in eq. (4) the transverse mass m_T^2 with Lambda mass m_Λ^2 whose value is taken to be $m_\Lambda = 1115.683$ MeV [8].

4 Modelling Lambda Fracture Functions

The fracture formalism relies on the assumption that leading particle production in the target-fragmentation region is a leading-twist process. The latter has been strikingly confirmed by experimental observation of hard diffraction at HERA [22, 23]. In the present context, however, the limited amount of data is often presented as Q^2 -integrated single-differential distributions, a fact which prevents any conclusion to be drawn. We only note that such hypothesis might be indirectly supported by the moderate value of the average Q^2 for the semi-inclusive reactions quoted in Tab. (1) and by the mild increase of the Lambda average multiplicity $\langle n(\Lambda) \rangle$ as a function Q^2 , as seen in data [18].

Although the scale dependence of fracture functions is predicted by perturbative QCD, these distributions still need to be modelled at some low scale and evolved to scales relevant to the experiments; the resulting free parameters controlling their input distributions can then be constrained by a fit to data. These distributions, however, depend upon the x_B and ζ variables and on the interacting parton flavour and therefore are expected to contain a large number of free parameters. In this respect, it would be possible to use as input the parton distributions and the fragmentation functions of Regge-based models, such as the quark-gluon string model (QGSM) of Ref. [24]. This would reduce the number of free parameters; in the present analysis, however, we have decided to use realistic parton distributions determined from fits to DIS experiments [20] and a completely free input parametrisation of the fragmentation functions in order to guarantee sufficient generality and flexibility. We will compare the QGSM and our best-fit parametrisations at the end of Section 5.

Since the hard scattering process occurs on time scales much shorter than spectator-fragmentation ones, we assume that, at an arbitrary low scale Q_0^2 , fracture functions factorise into a product of ordinary parton distributions $f_{i/p}(x_B, Q_0^2)$ and what we address as spectator-fragmentation functions $\tilde{D}_i^{\Lambda/p}(z)$

$$(1 - x_B) M_i^{\Lambda/p}(x_B, \zeta, Q_0^2) = M_i^{\Lambda/p}(x_B, z, Q_0^2) = f_{i/p}(x_B, Q_0^2) \tilde{D}_i^{\Lambda/p}(z), \quad i = q, \bar{q}, g. \quad (12)$$

We take advantage of the sea-valence decomposition offered by parton distributions of Ref. [20] to further decompose the valence parton contributions as

$$M_{q=u,d}^{\Lambda/p}(x_B, z, Q_0^2) = q_{val}(x_B, Q_0^2) \tilde{D}_{q_{val}}^{\Lambda/p}(z) + q_{sea}(x_B, Q_0^2) \tilde{D}_{q_{sea}}^{\Lambda/p}(z). \quad (13)$$

For the non-perturbative spectator-fragmentation function we choose a simple functional form of the type

$$\tilde{D}_i^{\Lambda/p}(z) = \overline{N}_i z^{\alpha_i} (1 - z)^{\beta_i}. \quad (14)$$

In order to minimise correlations between parameters, the normalisation coefficients in eq. (14) are defined as follows

$$\overline{N}_i = N_i \left[\int_0^1 dz z^{\alpha_i} (1-z)^{\beta_i} \right]^{-1}, \quad \alpha_i, \beta_i > -1, \quad (15)$$

and N_i are then used as free parameters in the fit. The inclusion of deuteron-target data in the fit requires the knowledge of neutron-to-Lambda fracture functions. As a first approximation we assume u - d isospin symmetry

$$\begin{aligned} M_d^{\Lambda/n}(x_B, z, Q^2) &= M_u^{\Lambda/p}(x_B, z, Q^2), \\ M_u^{\Lambda/n}(x_B, z, Q^2) &= M_d^{\Lambda/p}(x_B, z, Q^2). \end{aligned} \quad (16)$$

Limiting ourselves to the discussion of the valence region and indicating in parenthesis the flavour structure of the spectator system, we note that eqs. (16) imply

$$\tilde{D}_{u(ud)}^{\Lambda/p} = \tilde{D}_{d(ud)}^{\Lambda/n} \quad \text{and} \quad \tilde{D}_{d(uu)}^{\Lambda/p} = \tilde{D}_{u(dd)}^{\Lambda/n}. \quad (17)$$

Given the input distributions in eqs. (12,13), set at an initial scale $Q_0^2 = 0.5 \text{ GeV}^2$, we numerically solve the fracture-functions evolution equations in eq. (9) by using a finite-difference method in x_B -space in slices of ζ . We use the leading-order proton parton distribution of Ref. [20] and Λ fragmentation functions of Refs. [19] extracted taking into account target-hadron mass effects. For consistency, we follow the original evolution scheme of Ref. [20]. We evolve light-quarks fracture functions at leading-logarithmic accuracy within a fixed flavour-number scheme. Heavy-quarks effects are included in the running of the strong coupling at the heavy-quark mass thresholds and $\Lambda_{\text{QCD}}^{(n_f)}$ values are taken from Ref. [20].

As a final remark to this section we would like to discuss the impact of the inhomogeneous term in eq. (9) on the observables entering the fit. As a first step we have checked that, in the current region where the leading order semi-inclusive cross sections are proportional to the product of parton distributions and fragmentation functions, a reasonable description of μp data of Ref. [14] can be obtained both in shape and in normalisation by using parton distributions and fragmentation functions of Refs. [20] and Ref. [19], respectively. We then use fragmentation functions of Ref. [19] in the calculation of the inhomogeneous term appearing in eq. (9). At the observable level such term accumulates, as expected, at small $|x_F|$ as a result of the z shape of Lambda fragmentation functions. Moreover it contributes only at the percent level to the x_F distributions since it describes Lambda production from the fragmentation of radiated partons with transverse momentum greater than the minimum momentum transfer involved in the process, that is Q_0^2 . As such it only contributes to the small radiative tail of the Lambda p_t -spectrum.

The radiative contributions generated by the inhomogeneous term and the universality of fragmentation functions could be studied in detail in processes that do not show any leading particle effect, for example the production of anti-Lambdas [14] or light mesons [25] off protons, or in target-like Lambda production in a perturbative regime (*i.e.* with sufficiently large transverse momentum, $p_t \geq 1 \text{ GeV}$).

Reaction type	partial χ^2	# fitted points
νp [12]	4.77	5
νn [12]	3.25	5
νp [13]	6.36	8
$\bar{\nu} p$ [13]	9.08	8
μp [14]	9.90	8
μD_2 [14]	10.58	9
μD_2 [15]	0.20	3

Table 2: Partial χ^2 contributions and number of points in the fit for each data set.

$\tilde{D}_i^{\Lambda/p}$	N_i	α_i	β_i
u_{val}	0.046 ± 0.006	2.82 ± 1.19	0.39 ± 0.33
d_{val}	0.027 ± 0.006	$= \alpha_{u_{val}}$	1.28 ± 0.51
q_{sea}	0.078 ± 0.010	0	1.84 ± 0.63

Table 3: Best-fit values according to eq. (14).

5 Fitting procedure

Each of the assumed Lambda spectator-fragmentation functions in eq. (14) contains three free parameters (one normalisation and two exponents). Our fitting strategy is the following: we first tentatively assume as many different fragmentation functions as possible types of struck partons (valence or sea u , valence or sea d , other sea quarks, gluon). The observable $1/\sigma_{\text{DIS}} d\sigma^\Lambda/dx_F$ is then reconstructed via eq. (10) and the best-fit parameter values are determined using the MINUIT [26] program. We assume that the uncertainties on the cross sections combine statistical and systematic errors so that we use the simplest version of the χ^2 -function as a merit function, although this neglects correlations between data points (the number of the latter is rather limited and amounts to 46). We then study the eigenvalues and the eigenvectors of the fit covariance matrix to identify any parameters that are badly constrained by the fit. We fix them by making some assumptions about their values and we repeat the fit with the remaining parameters.

With the available data, for example, the fit can not constrain distinct sea-quark fracture functions. We therefore assume a common spectator-fragmentation function for all of them, $\tilde{D}_{q_{sea}}^{\Lambda/p}$. Moreover the fit is found to be insensitive to the choice of the gluon spectator fragmentation function. This is not unexpected since the gluon is coupled to electroweak probes only through higher orders. For this reason, we fix the gluon spectator-fragmentation functions to be equal to the sea one, $\tilde{D}_g^{\Lambda/p} = \tilde{D}_{q_{sea}}^{\Lambda/p}$, reducing the number of free parameters to nine. In such a fit the smallest eigenvalues of the Hessian matrix correspond to eigenvectors whose largest components are associated with the parameters α_i . The poor determination of such parameters can be partly associated to mass effects in the reconstruction of the observable in eq. (10) via eq. (4). The parameter $\alpha_{q_{sea}}$ is compatible with zero within errors so we fix it to this value. Furthermore, the parameters $\alpha_{u_{val}}$ and $\alpha_{d_{val}}$ are equal to each other within errors, so we assume $\alpha_{u_{val}} = \alpha_{d_{val}}$,

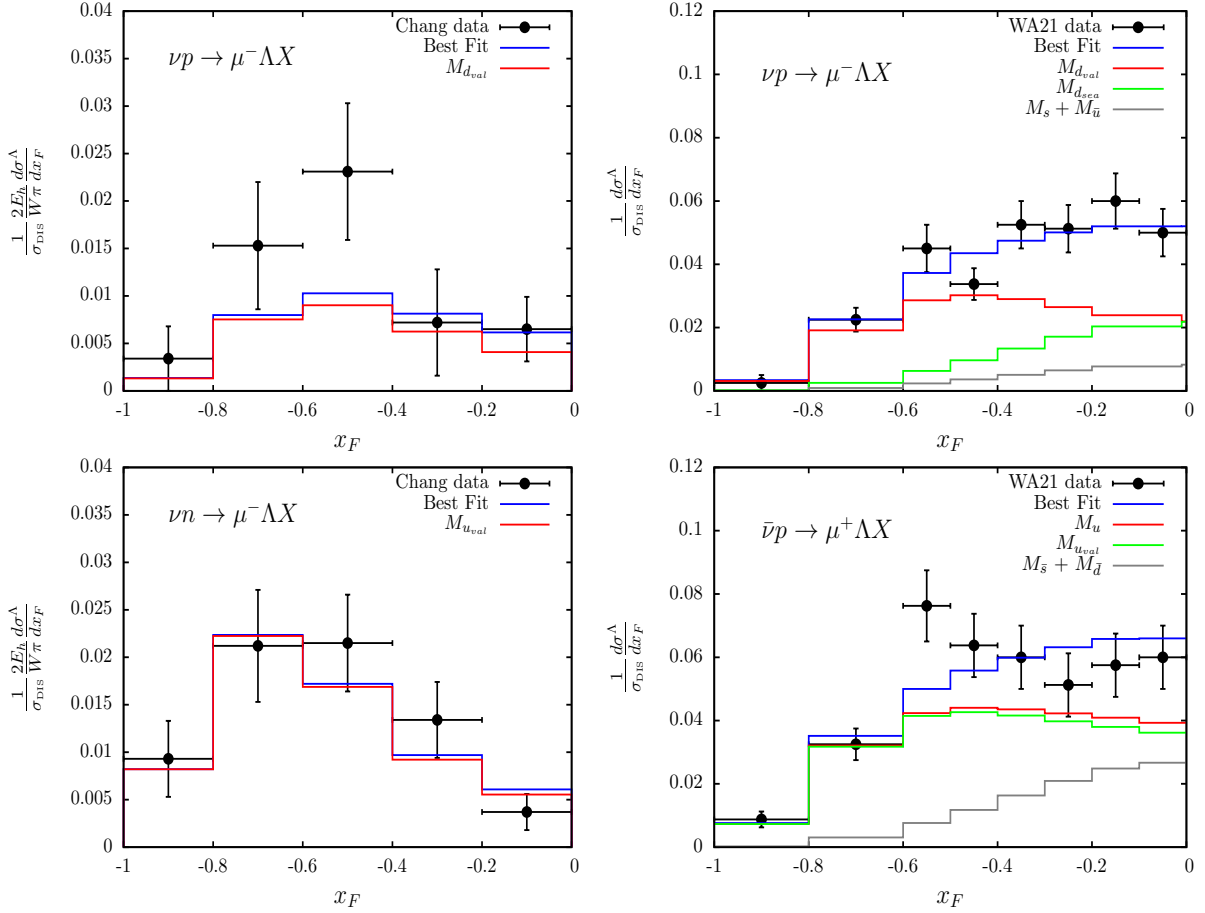


Figure 1: Best-fit predictions compared to normalised x_F distributions for charged current semi-inclusive Lambda cross-sections from Ref. [12] (left panels) and Ref. [13] (right panels). Various quark-flavour proton-to-Lambda fracture functions contributions are shown. Note the additional factor $2E_h/(\pi W)$ which multiplies the normalised cross-sections from Ref. [12].

reducing the number of free parameters to seven. Fixing some of the parameters to a definite value is indeed an arbitrary procedure. We can motivate this choice only a posteriori by noting that, when these parameters are optimised by the fit, the value of the χ^2 function is only marginally reduced. The best seven-parameter fit yields a $\chi^2/d.o.f. = 44.14/(46 - 7) = 1.13$. The partial χ^2 and the number of points included in the fit for each data set are displayed in Tab. (2). The results for the best-fit parameters are reported in Tab. (3) along with parameter errors as calculated by the MINUIT routine HESSE, which assumes a parabolic behaviour of the χ^2 function in parameter space around the minimum.

The best-determined parameters are the three normalisations, which implies that three independent distributions are in fact sufficient to handle the normalisation spread between the various data sets. The four parameters controlling the shape of the spectator functions have substantially larger uncertainties. The sources of the latter are primarily related to the intrinsic correlation between the α_i and β_i parameters introduced by the specific functional form as-

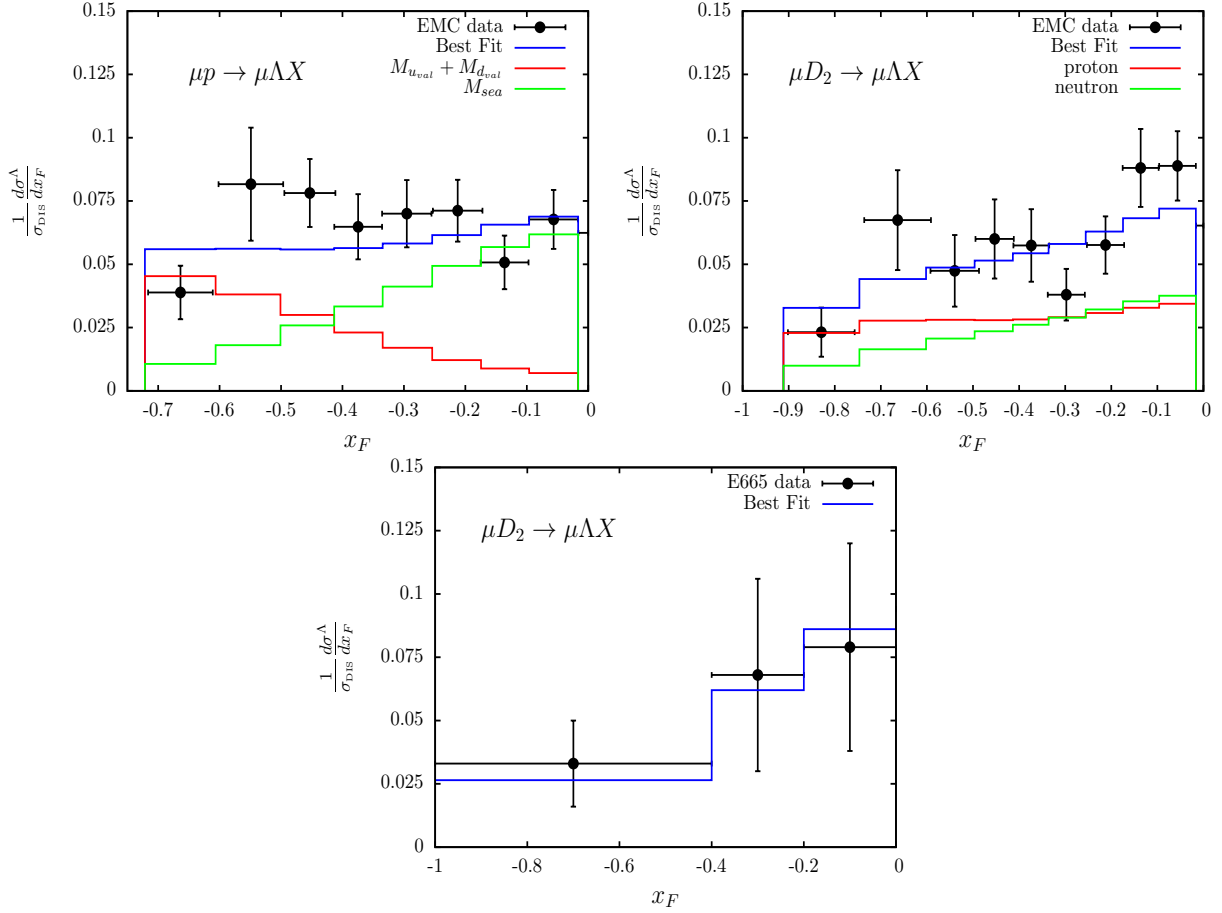


Figure 2: Best fit predictions compared to normalised x_F distributions for μp (left panel) and μD_2 (right panel) data from Ref. [14] and μD_2 (bottom panel) data from Ref. [15]. In the μp case valence- and sea-quark fracture functions contributions are separately shown. In the μD_2 case the proton- and neutron-target contributions are separately shown.

summed for the spectator functions in eq. (14). We also note that, at low centre-of-mass energy, where mass corrections introduced via eq. (4) are sizeable, a large portion of the x_F spectrum is controlled by the behaviour of the spectator functions in the neighbourhood of $z = 1$; the shape of the predicted spectrum is thus mainly determined by the β_i parameter alone. Therefore, parametrisations with more modulable behaviour at large z could improve the description of the x_F spectra. These improvements are probably marginal given the quality of the data used in this fit, but they might be necessary when dealing with higher quality data as presented, for example, in Ref. [18].

Given the stringent cut on the DIS selection, the data of Ref. [12] constrain the valence-quark fracture-function contributions, $M_{q_{\text{val}}}$, which in fact almost saturate the spectrum, as shown in the left column plots of Fig. (1). The plots in the first row of Fig. (1) show instead a normalisation tension between νp data from Ref. [12] and Ref. [13] which, however, can be tolerated in view of the partial χ^2 presented in Tab. (3). The plots in the second row show a

slight shape deformation in the predictions for νn data from Ref. [12] which is probably due to the normalisation constraint induced by $\bar{\nu}p$ data from Ref. [13] on the individual $M_{u_{val}}$ and $M_{q_{sea}}$ distributions. These results indeed indicate, as expected, that Lambdas are produced more abundantly and more forward by the fragmentation of ud -spectator system with respect to a uu -one.

We show in Fig. (2) the best-fit predictions for data from Ref. [14] and Ref. [15] for which the incident muon beam energy is significantly higher than neutrino and anti-neutrino ones. Quite interestingly, the spectrum at large $|x_F|$ is dominated by valence-quark fracture functions, as shown in the upper left panel of Fig. (4). The differences between $M_{u_{val}}$ and $M_{d_{val}}$ distributions is responsible for the different large $|x_F|$ behaviour on different targets, as shown in the upper right panel of Fig. (4). In these processes, characterised by higher values of $\langle W^2 \rangle$, Lambda-mass corrections play a less prominent role and therefore the z shape of the sea-quark fracture functions, as parametrised in Tab. (3), are clearly visible in the plots. The quality of the fit is stable against variations of the arbitrary scale Q_0^2 at which fracture functions are factorised into parton distributions and spectator fragmentation functions. The χ^2 function, in fact, shows a very mild dependence on Q_0^2 as the latter is varied below the measured range between 0.5 and 1.0 GeV².

We wish to conclude this Section by comparing our best-fit parametrisations for the spectator-fragmentation functions with the analogous ones used in the QGS model [24]. This is possible since both models assume a factorised input at some low scale, eq. (12), and similar functional forms for $\tilde{D}_i^{\Lambda/p}(z)$, eq. (14). The comparison however should be performed with some care: valence- and sea-quarks distributions in the QGSM have all the same x distribution, at variance with the ones used in the present analysis [20]. Furthermore the scale at which the QGSM model is assumed to be valid does not necessarily match the Q_0^2 scale used in the fit. This is particularly important since the scale Q_0^2 determines the relative weight of sea- and valence-parton distributions appearing in the fracture function decomposition in eq. (13) and therefore the $\tilde{D}_i^{\Lambda/p}(z)$ themselves. Comparisons for the fragmentation functions are presented in Fig. (3). The Lambda spectrum at large $|x_F|$ is driven by the large- z behaviour of $M_{u_{val}}$ and $M_{d_{val}}$. We can then compare directly the best-fit β_i parameters with the analogous ones in the QGS model. They can be read out from the D_{1ud}^Λ and D_{1uu}^Λ terms appearing in the appendix of Ref. [24] and, in our notation, are given by $\beta_{u_{val}} = 0.5$ and $\beta_{d_{val}} = 1.5$. These values, within errors, are in agreement with the best-fit parameters extracted in this analysis and listed in Tab. (3). The behaviour of the D_{1ud}^Λ and D_{1uu}^Λ terms at low z is significantly softer, $\alpha_{q_{val}} = 1$, than in our model, $\alpha_{q_{val}} = 2.82$. In our model, on the other hand, sea-quarks spectator fragmentation-functions are harder, $\beta_{q_{sea}} = 1.8$ and $\alpha_{q_{sea}} = 0$, with respect to the QGSM predictions, for which $\beta_{q_{sea}} = 2 \div 3.5$ depending on the sea-quarks flavour and $\alpha_{q_{sea}} = -1$. The main differences between the two models therefore appear at intermediate and low z where there is no evidence in our best-fit parametrisations of the z^{-1} behaviour as predicted by the QGSM. Such different behaviour is determined by the value of the $\alpha_{q_{sea}}$ parameter which, due to the reduced sensitivity at low z caused by sizeable Lambda-mass corrections, was loosely determined by the fit and therefore fixed to zero. With these respect semi-inclusive DIS data at higher centre-of-mass energy will better constrain the spectator fragmentation functions at small z and test QGSM predictions.

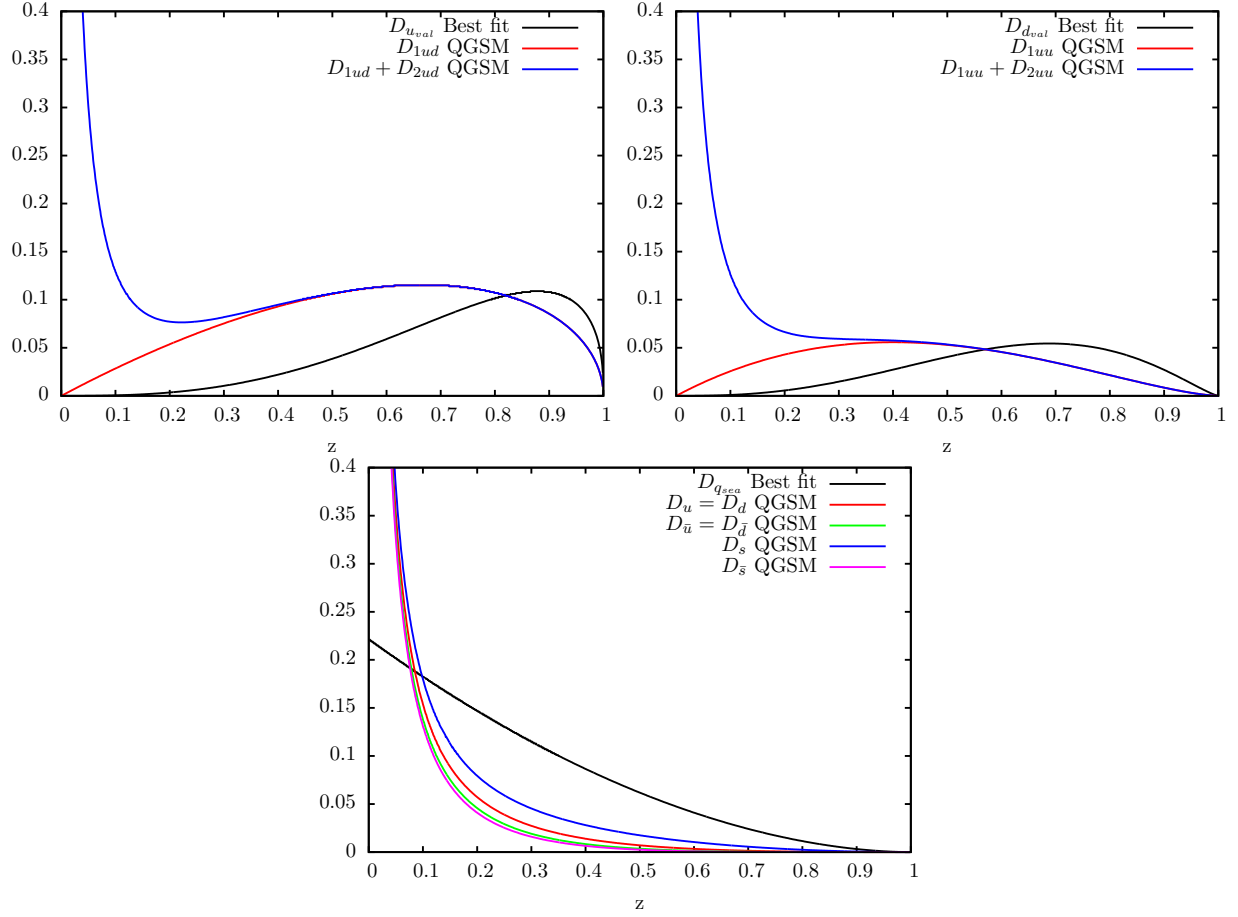


Figure 3: Spectator fragmentation functions from our best fit and from the QGS model.

6 Predictions

In this last section we wish to discuss the degree of predictivity of the model. It is of particular importance to determine to which extent the model is able to reproduce x_F distributions coming from data not included in the fit or observables other than the ones used in the fit. This comparison will eventually pinpoint sectors of the model which may need to be improved. The comparison with the x_B or Q^2 distributions require the reconstruction of the current fragmentation term, which is obtained with the semi-inclusive version of eqs. (5,6,7) where fracture functions are substituted by appropriate products of parton distributions and fragmentation functions. Such term has been estimated to leading order by using the parton distributions of Ref. [20] and the fragmentation functions of Ref. [19].

As a first example, we consider Lambda production in neutrino- and anti-neutrino-induced charged-current DIS on proton and neutron targets [27]. These data provide full flavour discrimination of the spectator system and can be used to test the assumptions made in eq. (16). Unfortunately, the x_F distributions for these data are presented in Ref. [27] as histograms without errors. In a subsequent paper by the same collaboration [28], the Lambda yields are updated

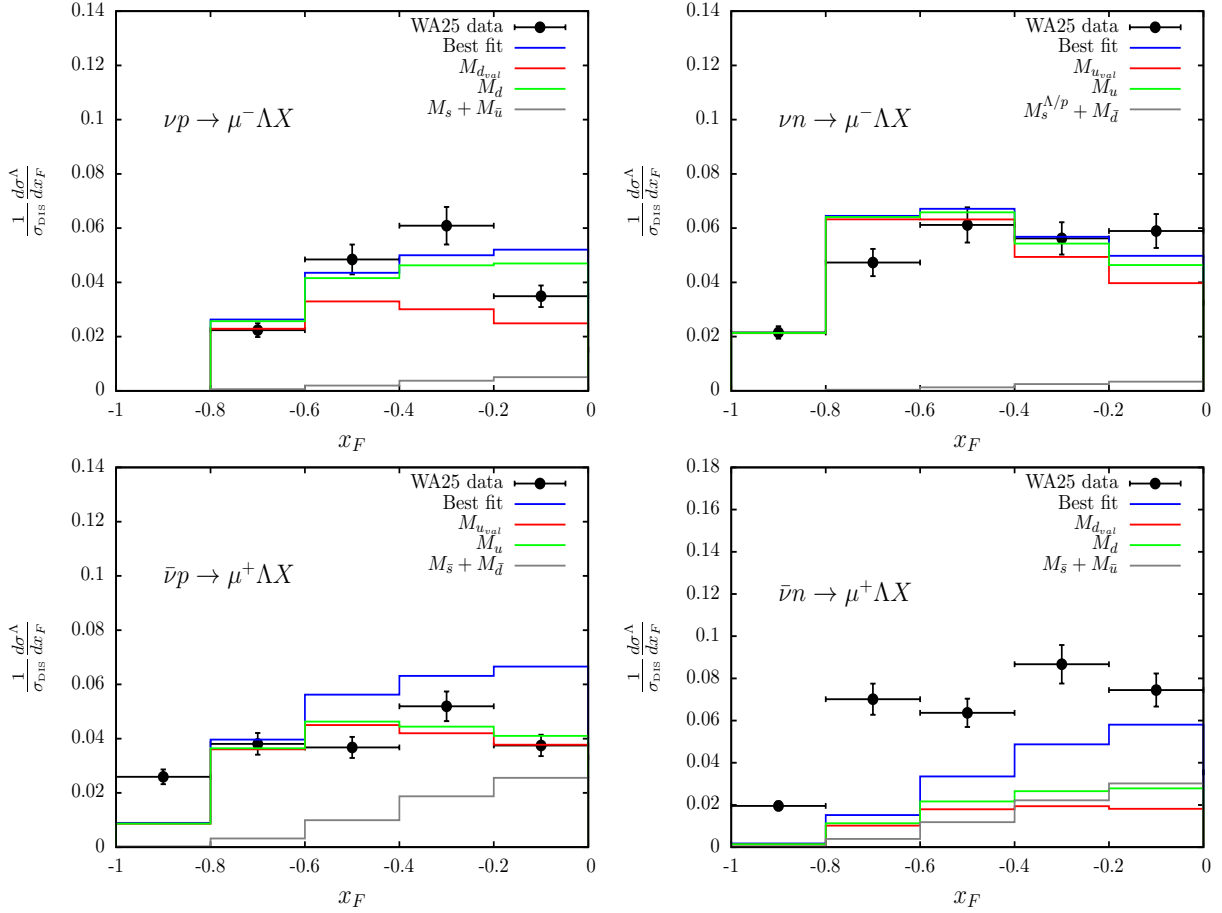


Figure 4: Best-fit predictions compared to normalised x_F -distributions for charged current semi-inclusive Lambda cross-sections from Refs. [27, 28]. Various quark-flavour proton-to-Lambda fracture functions ontributions are shown.

but no x_F distributions are given.

In order to gauge the agreement of the best-fit model predictions with these data, we have assessed the errors in the following way. First the histograms from Ref. [27] have been scaled down to the updated yields of Ref. [28] assuming no change in their shape. Then we have assumed that the relative errors of the x_F distributions in each x_F bin are equal. This in turn implies that they are respectively equal to the relative error on the corresponding Lambda yield. This procedure guarantees that upon integration over x_F , the experimental yield and its error are correctly recovered. The best-fit predictions are compared to data in Fig. (4). We note that, in general, the cross sections on proton target are fairly reproduced in normalisation, as expected, since the Lambda yields in $\bar{\nu}p$ - and νp -scattering of Ref. [28] are in agreement within errors with those of data included in the fit [12, 13]. The predicted distributions do not reproduce the turn-over at low $|x_F|$ as seen in data, reflecting the shape of the fitted data [12, 13], as shown in the right-hand-side panels of Fig. (1). The comparison with neutron-target data reveals that, in this case, the model does not perform equally well. In particular, the νn cross sections peaks

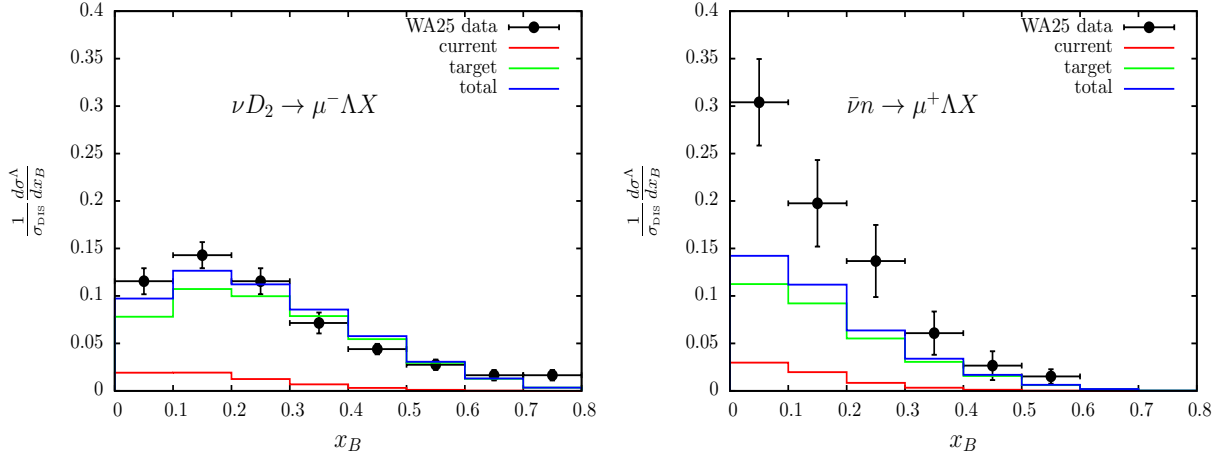


Figure 5: Normalised x_B distributions in νD_2 (left panel) and $\bar{\nu}n$ (right panel) scattering. Data are taken from Ref. [28].

at too large values of $|x_F|$, a behaviour mainly driven by the νn data of Ref. [12] and illustrated in the lower left panel of Fig. (1). While all these distributions are quite well reproduced in normalisation, the model significantly underestimates the $\bar{\nu}n$ -scattering data. In this case, the disagreement between data and theory might indicate that some of the assumptions on fracture-function parametrisations used in the fit, for example $\tilde{D}_{u(dd)}^{\Lambda/n} = \tilde{D}_{d(uu)}^{\Lambda/p}$ as well as considering a common spectator fragmentation function for all sea-quarks, could be relaxed, as we discuss in the following.

The same data are presented in Fig. (5) in terms of normalised x_B distributions [28]. We remind the reader that we integrate over the x_B variable in the reconstruction of the x_F distributions. Therefore the comparison of the x_B distributions with data constitutes a non-trivial test for the model. Excellent agreement is found for the νD_2 cross section, both in shape and in normalisation. On the other hand, model predictions for the $\bar{\nu}n$ cross section fail to reproduce experimental distributions, as in the corresponding x_F distribution in the lower right panel of Fig. (4). Since the $\bar{\nu}n$ cross section significantly exceeds the νD_2 only in the smallest x_B bin, the hypothesis that target Lambdas could be more abundantly produced in $\bar{\nu}\bar{s}$ -scattering rather than in νs -scattering was originally formulated in Ref. [28], based on the idea that, in the sea-quark region, $\bar{\nu}\bar{s}$ -scattering leaves the correct hypercharge in the target spectator. In our framework, this hypothesis would directly translate into an asymmetry of the spectator fragmentation functions in the strange sector, $\tilde{D}_{\bar{s}}^{\Lambda/p} \neq \tilde{D}_s^{\Lambda/p}$. The cross sections used in the regression however can not individually constrain $\tilde{D}_{\bar{s}}^{\Lambda/p}$ and $\tilde{D}_s^{\Lambda/p}$, because of the linear combinations of sea-quark fracture functions appearing in the structure functions in eqs. (5,6,7).

In this respect, the associated production of target Lambdas in dimuon (anti-)neutrino-nucleon deep-inelastic scattering, $\nu N \rightarrow \mu^- \mu^+ \Lambda X$ and $\bar{\nu} N \rightarrow \mu^+ \mu^- \Lambda X$, could represent an alternative sensitive test of the latter hypothesis. In the corresponding parton sub-process, $W^+ s \rightarrow c$ and $W^- \bar{s} \rightarrow \bar{c}$, a (anti-)charm, produced by a charged current, semileptonically decays in the current fragmentation region into a final-state, secondary, muon. Given the small off-diagonal quark-mixing CKM matrix elements and the known parameters of charm quarks decay, the

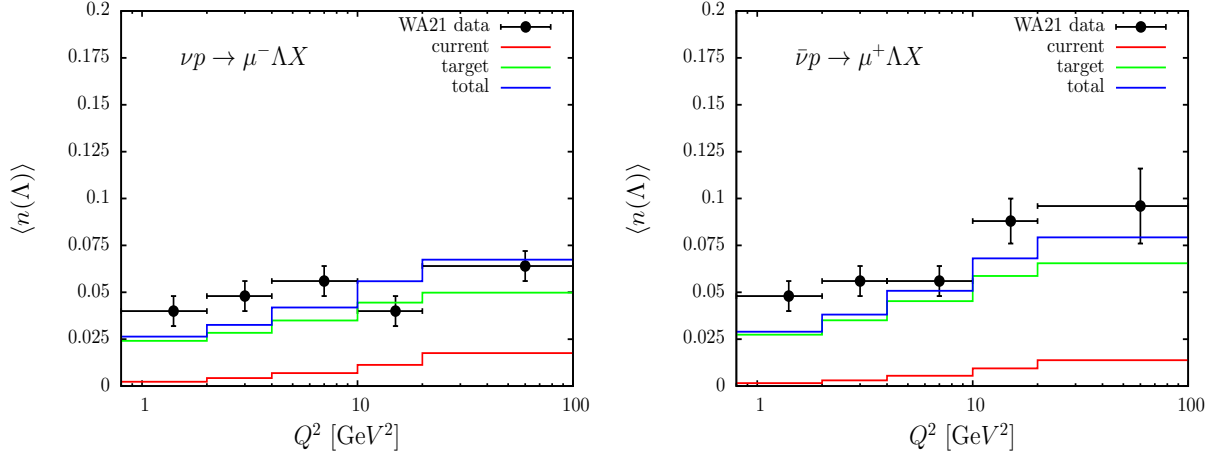


Figure 6: Lambda average multiplicity as a function of Q^2 in νp (left panel) and $\bar{\nu} p$ (right panel) scattering. Current and target contributions are separately shown. Data are from Ref. [13].

detection of the additional muon allows to probe directly the (anti-)strange component of the nucleon [29]. Therefore, in this class of events, the additional detection of a Λ hyperon in the target fragmentation could test the proposed asymmetry.

We conclude by showing in Fig. (6) the model predictions for the averaged Lambda multiplicity as a function of Q^2 in νp and $\bar{\nu} p$ charged-current SIDIS cross sections. Although the x_F distributions from this data set [13] have been already used in the fit and therefore agreement in normalisation might be expected, the model is able to reproduce reasonably well the observed Q^2 dependence, with a tendency to undershoot the data at the lowest value of Q^2 . Since the Q^2 dependence built in the model via fracture-function evolution equations can be considered one of the most stringent predictions of the underlying theoretical framework, the reasonable agreement between data and predictions can be considered the first step towards a conclusive validation of the perturbative framework. The validation procedure and the model itself would, in fact, highly benefit from the constraints imposed by multi-differential distributions. Cross sections at fixed x_B and x_F as a function of Q^2 , for example, could give access, through scaling violations, to the presently unconstrained gluon fracture function, $M_g^{\Lambda/p}(x_B, z, Q^2)$.

7 Summary and conclusions

In this paper we have analysed experimental data on the production of Lambda hyperons in the SIDIS target fragmentation region in terms of fracture functions. A model for the latter has been proposed and the free parameters appearing in the input distributions have been fixed by performing a fit to a variety of neutral- and charged-current semi-inclusive DIS cross sections. The main features seen in the data can be fairly reproduced by the model. In particular the spectator-fragmentation functions associated with the removal of valence quarks populate the very forward part of the x_F -spectrum at large and negative values of x_F . On the other hand, the sea-quarks contribution is concentrated at small and negative values of x_F . The predictions based

on the model are in fair agreement with data not included in the fit and with observables depending on variables which are integrated over in the analysis, especially the Q^2 dependence of the Lambda multiplicity, which is a stringent test of the underlying theoretical framework. Although further tests and additional experimental informations are necessary to validate and eventually improve the model, it may be used to quantitatively investigate spectator-fragmentation mechanisms within a perturbative QCD approach. Since higher-order calculations are available in the literature, the analysis can be extended to next-to-leading order accuracy. The model can be easily generalised to take into account Lambda polarisation allowing spin-transfer studies [30] in the target region and it may find application in the estimation of nuclear corrections to target fragmentation.

Acknowledgements

We gratefully acknowledge M. Stratmann and S. Albino for providing us with their fragmentation-function routines. We especially acknowledge D. Naumov for interesting discussions related to backgrounds in Lambda production in DIS and for providing us the neutrino flux parametrisations. We wish to thank the organizers of the Workshop "Strangeness polarization in semi-inclusive and exclusive Lambda production" held in ECT*, Trento, in October 2008 and all the participants for stimulating discussions on this topic. We finally thank Laurent Favart, Dmitry Naumov, Jean-Ren  Cudell and Luca Trentadue for a critical reading of the manuscript prior to submission.

References

- [1] M. Basile *et al.*, *Nuovo Cim.* **A66** (1981) 129.
- [2] L. Trentadue and G. Veneziano, *Phys. Lett.* **B323** (1994) 201.
- [3] Yu. L. Dokshitzer, *Sov. Phys. JETP* **46** (1977) 641;
V. N. Gribov and L. N. Lipatov, *Sov. J. Nucl. Phys.* **15** (1972) 438;
G. Altarelli and G. Parisi, *Nucl. Phys.* **B126** (1977) 298.
- [4] D. Graudenz, *Nucl. Phys.* **B432** (1994) 351.
- [5] J. C. Collins, *Phys. Rev.* **D57** (1998) 3051.
- [6] M. Grazzini, L. Trentadue and G. Veneziano, *Nucl. Phys.* **B519** (1998) 394.
- [7] J. Levelt and P. J. Mulders, *Phys. Rev.* **D49** (1994) 96.
- [8] J. Beringer *et al.* (Particle Data Group), *Phys. Rev.* **D86** (2012) 010001.
- [9] E. Konishi, A. Ukawa and G. Veneziano, *Nucl. Phys.* **B157** (1979) 45.
- [10] D. de Florian, C. A. Garcia Canal and R. Sassot, *Nucl. Phys.* **B470** (1996) 195.

- [11] D. de Florian and R. Sassot, *Nucl. Phys.* **B488** (1997) 367.
- [12] C. C. Chang *et al.*, *Phys. Rev.* **D27** (1983) 2776.
- [13] G. T. Jones *et al.* (WA21 Collaboration), *Z. Phys.* **C57** (1993) 197.
- [14] M. Arneodo *et al.* (EMC Collaboration), *Z. Phys.* **C34** (1987) 283.
- [15] M. R. Adams *et al.* (E665 Collaboration), *Z. Phys.* **C61** (1994) 539.
- [16] A. Airapetian *et al.* (Hermes Collaboration), *Eur. Phys. J.* **A47** (2011) 113.
- [17] N. M. Agababyan *et al.* (SKAT Collaboration), *Phys. Atom. Nucl.* **70** (2007) 1731.
- [18] P. Astier *et al.* (NOMAD Collaboration), *Nucl. Phys.* **B621** (2002) 3.
- [19] S. Albino, B. A. Kniehl and G. Kramer, *Nucl. Phys.* **B803** (2008) 42.
- [20] M. Glück, E. Reya and A. Vogt, *Z. Phys.* **C67** (1995) 433.
- [21] P. Astier *et al.* (NOMAD Collaboration), *Nucl. Instrum. Meth.* **A515** (2003) 800.
- [22] M. Derrick *et al.* (ZEUS Collaboration), *Phys. Lett.* **B315** (1993) 481.
- [23] T. Ahmed *et al.* (H1 Collaboration), *Nucl. Phys.* **B429** (1994) 477.
- [24] A. B. Kaidalov and O. I. Piskunova, *Z. Phys.* **C30** (1986) 145.
- [25] M. Osipenko *et al.* (CLAS Collaboration), *Phys. Rev.* **D80** (2009) 032004.
- [26] F. James and M. Roos, *Comput. Phys. Commun.* **10** (1975) 343.
- [27] D. Allasia *et al.* (WA25 Collaboration), *Nucl. Phys.* **B224** (1983) 1.
- [28] D. Allasia *et al.* (WA25 Collaboration), *Phys. Lett.* **B154** (1983) 231.
- [29] S. Alekhin, S. Kulagin and R. Petti, *Phys. Lett.* **B675** (2009) 433.
- [30] J. R. Ellis *et al.*, *Eur. Phys. J.* **C52** (2007) 283.